

Cloud Feedback on Earth's Long-term Climate Simulated by a Near-global Cloud-permitting Model

Mingyu Yan¹, Jun Yang¹, Yixiao Zhang^{1,2}, Han Huang^{1,3}

¹Laboratory for Climate and Ocean-Atmosphere Studies, Department of Atmospheric and Oceanic Sciences, School of Physics, Peking University, Beijing 100871, China

²Now at Department of Earth Atmospheric and Planetary Sciences, Massachusetts Institute of Technology, 77 Massachusetts Avenue, Cambridge, MA 02139, USA

³Now at Department of Atmospheric and Oceanic Sciences, McGill University, Montreal, Canada

Key Points:

- A near-global cloud-permitting model with a resolution of $10\text{ km} \times 14\text{ km}$ is employed to test whether there is a long-term cloud feedback.
- The cloud feedback does have a net cooling effect when the Sun becomes brighter and meanwhile the CO_2 concentration decreases.
- These results confirm that cloud feedback is a part of the solution to the faint young Sun problem but its magnitude is relatively small.

Abstract

The Sun becomes brighter with time, but Earth’s climate is roughly temperate for life during its long-term history; for early Earth, this is known as the Faint Young Sun Problem (FYSP). Besides the carbonate-silicate feedback, recent researches suggest that a long-term cloud feedback may partially solve the FYSP. However, the general circulation models they used cannot resolve convection and clouds explicitly. This study re-investigates the clouds using a near-global cloud-permitting model without cumulus convection parameterization. Our results confirm that a stabilizing shortwave cloud feedback does exist, and its magnitude is $\approx 6 \text{ W m}^{-2}$ or 14% of the energy required to offset a 20% fainter Sun than today, or $\approx 10 \text{ W m}^{-2}$ or 16% for a 30% fainter Sun. When insolation increases and meanwhile CO_2 concentration decreases, low-level clouds increase, acting to stabilize the climate by raising planetary albedo, and vice versa.

Plain Language Summary

The emergence and evolution of life require a relatively stable climate environment. In the solar system, life has been found only on Earth and appeared since about four billion years ago. The underlying mechanisms for maintaining the long-term climate on Earth is an important question but the answer is not completely clear. In this study, we re-investigate a recently proposed mechanism, a stabilizing cloud feedback, using a high-resolution cloud-permitting model in a near-global domain. Our simulations confirm that a stabilizing cloud feedback does exist, but its magnitude is relatively small.

1 Introduction

The luminosity of the Sun increases with time, and the solar constant in the Archean Eon was 20–30% lower than that today (Gough, 1981). If other climate-controlling factors were the same as present, Earth would have been in a globally ice-covered snowball state during the Archean (Sagan & Mullen, 1972), but much evidence indicates that there was surface liquid water (Feulner, 2012). Hence, there should be some factors compensating for this discrepancy (Sagan & Mullen, 1972; Feulner, 2012; Charnay et al., 2020), and it is one of the most important problems on Earth’s long-term climate (Pierrehumbert, 2010). A number of studies show that biogeochemical feedbacks, such as the carbonate-silicate weathering cycle, are key to stabilizing the climate. The increase of greenhouse gas contents, such as CO_2 and CH_4 , is likely responsible for the FYSP (e.g., Wolf and Toon (2013); Byrne and Goldblatt (2014); Le Hir et al. (2014)). Other factors or feedbacks may have also contributed to solving this problem, such as a different atmospheric pressure, a less continent coverage, $\text{N}_2\text{-H}_2$ collision-induced warming, and a stronger tidal heating induced by the closer Moon (Goldblatt et al., 2009; Rosing et al., 2010; Goldblatt & Zahnle, 2011; Wordsworth & Pierrehumbert, 2013; Heller et al., 2021). A recent study of Goldblatt et al. (2021) suggested that a long-term cloud feedback exists and it could also be a part of the solution to the FYSP.

Clouds are one of the key factors that determine planetary climate. For low-level clouds, the cooling effect dominates; but for high-level clouds, the greenhouse warming effect dominates (Hartmann, 2005; Pierrehumbert, 2010). Goldblatt and Zahnle (2011) explored how clouds could resolve the FYSP in one-dimensional (1D) radiative-transfer simulations. They showed that a maximum radiative effect change of 15 W m^{-2} can be traced to a plausible low-level cloud reduction or high-level cloud increase. Using 3D GCMs, Charnay et al. (2013) and Wolf and Toon (2013) focused on the Archean Eon, and they found that the changes of clouds have a warming effect on the surface, mainly due to the reduction of low-level clouds. Goldblatt et al. (2021) systematically studied the cloud feedback using two GCMs: CAM4 and CAM5. They kept almost the same global-mean surface temperature ($|\Delta T| < 0.5 \text{ K}$) by increasing solar constant and meanwhile decreasing CO_2 concentration. Their work showed that shortwave cloud feedback has a stabilizing effect on the long-term

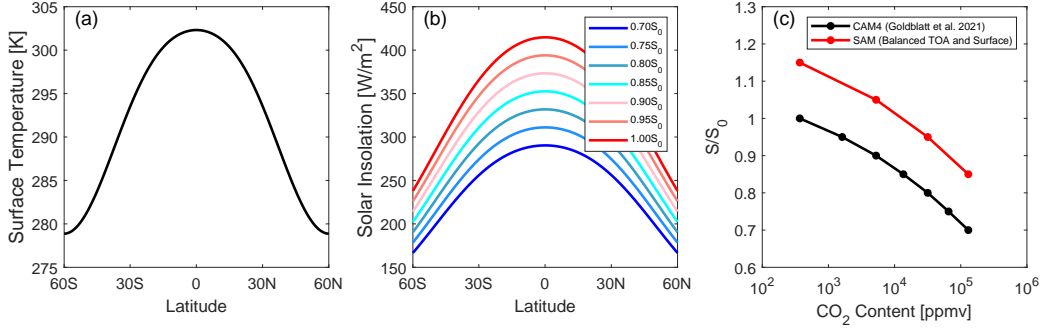


Figure 1. (a) Zonal-mean sea surface temperature in fixed SST simulations, (b) solar insolation distribution, and (c) CO₂ mixing ratio and insolation in different simulations.

climate, and it can offset 20 W m^{-2} or 40% in percentage of the required forcing when the insolation decreases from 1.0 to 0.8 times modern value. Below, we will show that they have overestimated the strength of the shortwave cloud feedback because the direct effect of varying solar radiation on the magnitude of shortwave cloud radiative effect without any change of cloud properties was not excluded. After subtracting this part, the magnitude of the shortwave cloud feedback in CAM4 is 8.6 W m^{-2} or 18.5% (see Section 3.1).

The horizontal grid sizes of GCMs are always larger than $\approx 100 \text{ km}$, but the sizes of convection and clouds are in the order of $\mathcal{O}(1\text{--}10) \text{ km}$ or even less, so that empirical convection and cloud parameterizations are necessary for GCMs. However, for GCMs, cloud feedback is the largest uncertainty source, leading to significant inter-model differences (e.g., Soden and Held (2006); Vial et al. (2017)). Therefore, it is important to use higher-resolution models or models with different parameterization schemes to re-examine the long-term cloud feedback proposed in Goldblatt et al. (2021). One method is using a cloud-resolving model that has a resolution of $\mathcal{O}(1) \text{ km}$ or smaller, but unfortunately, global-scale cloud-resolving simulations are far beyond present computation resources, especially when long-time integration and multiple experiments are required. Here, we use a cloud-permitting version with a resolution of $\approx 10 \text{ km}$, which is coarser than cloud-resolving models but much finer than GCMs, to re-simulate the clouds and the cloud feedback.

2 Model Descriptions and Experimental Designs

We run a series of simulations with the version 6.11.6 of the System for Atmosphere Modeling (SAM, Khairoutdinov and Randall (2003)). Anelastic momentum equations are used to explicitly resolve non-hydrostatic flows instead of the hydrostatic approximation used in GCMs. Radiation scheme is the same as the Community Atmosphere Model version 3 (CAM3) (Collins et al., 2006), and it is the same as that used in the CAM4 simulations of Goldblatt et al. (2021). There are still parametrizations in SAM that are used to calculate microphysics and sub-grid fluxes. Microphysics parameterization is based on a simple one-moment scheme, and a Smagorinsky-type closure scheme is used to calculate subgrid-scale fluxes (Khairoutdinov & Kogan, 1999; Khairoutdinov & Randall, 2003).

We use an aquaplanet mode, which means there is no land, and the northern and southern hemispheres are symmetric. The horizontal resolution is $\approx 14 \text{ km}$ in latitude and $\approx 10 \text{ km}$ in longitude, and the domain size corresponds to 60°S to 60°N in latitude and 0° to 180° in longitude. Rigid boundary conditions are used at y boundaries, and periodic boundary conditions are used at x boundaries. There are 38 vertical levels up to $\approx 35 \text{ km}$. The lowest mid-layer level is at 35 m , and the vertical grid spacing is $\approx 80 \text{ m}$ between the

two lowest levels and gradually increases to 1500 m above 10 km. A sponge layer is included above 28 km to reduce the reflection of gravity waves near the model top.

Letting sea surface temperature (SST) be interactive in a near-global domain comes with a huge computational cost, so we prescribe the SST. The spatial pattern of the specified SST is based on modern Earth, but it is zonally uniform and hemispherically symmetric (Figure 1a). We neglect diurnal and seasonal cycles, and set the distribution of solar insolation to be zonally uniform but latitude dependent (Figure 1b). For simplicity, the concentrations of ozone are set to 10^{-7} g g $^{-1}$ for all layers, and there is no other trace gas. Besides, cartesian geometry is used in SAM.

We did seven experiments by changing CO $_2$ concentration and solar constant synchronously (black line in Figure 1c). These experiments are respectively labeled as 0.70S $_0$, 0.75S $_0$, 0.80S $_0$, 0.85S $_0$, 0.90S $_0$, 0.95S $_0$, and 1.00S $_0$. The choices of insolation and CO $_2$ concentration are based on Goldblatt et al. (2021), in which a coupled slab ocean was employed and the obtained global-mean surface temperatures are nearly the same although the equator-to-pole surface temperature gradients change somewhat. For each experiment, the last 30 days are used in the following analyses (Figure S1). The details of these simulations are shown in Text S1.

Hourly-mean cloud fraction, precipitation, and precipitable water in the modern Earth simulation (1.00S $_0$) show that the key characteristics, such as the Intertropical Convergence Zone (ITCZ) and mid-latitude baroclinic clouds, can be well simulated in the cloud-permitting framework (Figure S2). However, there are some less realistic features, which were also noted in Bretherton and Khairoutdinov (2015). For example, the differences between continental clouds and oceanic clouds are not simulated because of the employed aquaplanet mode, and neither seasonal cycle nor diurnal cycle is simulated because of the fixed solar radiation and SST. Moreover, as we set the boundaries at 60°S(N), a lot of clouds are trapped near the boundary walls; these clouds are mostly advected from lower latitudes and trapped by the walls; if there were not these boundaries, clouds will further flow to higher latitudes and then precipitate to the surface.

Note that energy budgets at the top of the atmosphere (TOA) and the surface are not balanced because we prescribe SSTs. To decrease the energy imbalances of the TOA and surface, we re-do four experiments (0.70S $_0$, 0.80S $_0$, 0.90S $_0$, and 1.00S $_0$) with the solar constants increasing to respectively 0.85, 0.95, 1.05, and 1.15 S $_0$, and meanwhile the CO $_2$ concentrations are unchanged (Figure S3 and red line in Figure 1c). Besides, we also add two slab ocean runs (see Text S1, Figure S4). In these experiments, the energy imbalances at the TOA and surface decrease to be less than 3 W m $^{-2}$ (Figures S3 and S4).

3 Results

3.1 Cloud Feedback

When insolation increases and meanwhile CO $_2$ concentration decreases, global-mean low-level cloud fraction significantly increases, high-level cloud fraction slightly decreases, and middle-level cloud fraction is almost unchanged (Figure 2b). The water paths of clouds at different levels show the same trends as the cloud fractions (Figure 2c). Moreover, the same trends of cloud fractions and cloud water paths can be found in the energy-balanced fixed-SST simulations and also in the slab ocean simulations (Figure 3).

The increase of low-level clouds can reflect more insolation to space, leading to a larger planetary albedo (Figure 2a). For example, comparing the 0.80S $_0$ case and the 1.00S $_0$ case, the planetary albedo increases from 0.36 to 0.38, and the magnitude of shortwave cloud radiative effect increases from 45.1 to 64.0 W m $^{-2}$ (Figure 2d). The change of the shortwave cloud radiative effect is contributed by two parts, one is from the change of the solar radiation without any change of the cloud properties, and the other one is from the change of the cloud

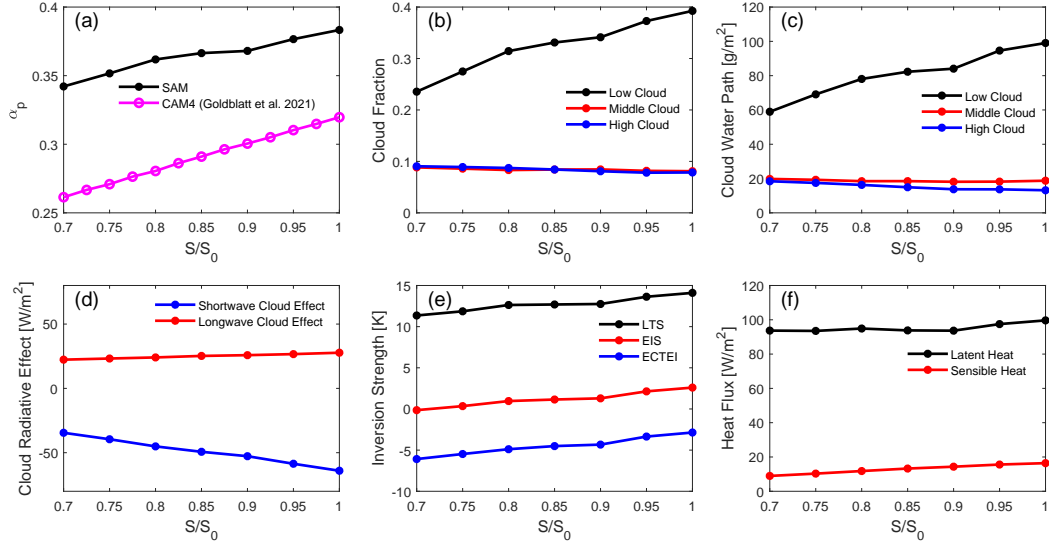


Figure 2. Results under different solar radiations and corresponding CO_2 concentrations. (a) Global-mean planetary albedo in our SAM simulations (black), (b) cloud fractions of low-level (black), middle-level (red), and high-level clouds (blue), (c) same as (b) but for cloud water paths, (d) shortwave (blue) and longwave (red) cloud radiative effects, (e) inversion strength indexes: lower tropospheric stability (LTS; black), estimated inversion strength (EIS; red), and estimated cloud-top entrainment index (ECTEI; blue; see Text S3 in the Supporting Information online), and (f) surface latent (black) and sensible (red) heat fluxes. The low-level cloud fraction in (b) is defined as the fraction of grids with vertically-integrated cloud water path between surface and 700 hPa exceeding 0.02 kg m^{-2} (Khairoutdinov & Randall, 2003). Likewise, the middle-level and high-level cloud fractions correspond to the vertically-integrated cloud water path of 700 to 400 hPa and above 400 hPa. In (a), the CAM4 simulation results of Goldblatt et al. (2021) (magenta) are included for comparisons.

properties without any change of solar radiation. The albedo of the $1.00S_0$ case is 0.38, so there should be $\approx 43.6 (= 1361.3/3.87 \times (1.00 - 0.38) \times (1.0 - 0.8)) \text{ W m}^{-2}$ less solar radiation absorbed when the solar constant is 80% of the modern Earth. Note that the denominator is 3.87 rather than 4.0; this is because the model uses Cartesian geometry rather than spherical geometry and meanwhile the polar regions are not simulated. When the $1.00S_0$ case is chosen as the baseline, the shortwave cloud feedback is $-45.1 - (-64.0) \times 0.8/1.0 = 6.1 \text{ W m}^{-2}$. In percentage, it is 14.0% ($= 6.1/43.6$). Another method for calculating the shortwave cloud feedback is shown in Text S2, and its value is 6.0 W m^{-2} . For a solar constant of 70% of the modern value, the strength of the shortwave cloud feedback is 10.3 W m^{-2} or 15.7%. The magnitude of the shortwave cloud feedback is similar to Wolf and Toon (2013), in which it can contribute $\approx 9.6 \text{ W m}^{-2}$ or 21% when the Sun is 20% dimmer (Figure 4, Charnay et al. (2020)).

In the CAM4 simulations of Goldblatt et al. (2021), the shortwave cloud radiative effects are -33.4 and -52.5 W m^{-2} , and the planetary albedos are 0.28 and 0.32, for the $0.80S_0$ and $1.00S_0$ cases, respectively (Figure S5). There should be $46.5 (= 1367.0/4.0 \times (1.00 - 0.32) \times (1.0 - 0.8)) \text{ W m}^{-2}$ less solar radiation absorbed in the $0.80S_0$ case. The shortwave cloud feedback equals $-33.4 - (-52.5) \times 0.8/1.0 = 8.6 \text{ W m}^{-2}$, or 18.5% ($= 8.6/46.5$) in percentage. For $0.70S_0$, the strength of the shortwave cloud feedback is 10.7 W m^{-2} or 15.4% (Figure 4). Note that the estimated magnitudes of the shortwave cloud feedback in Goldblatt et al.

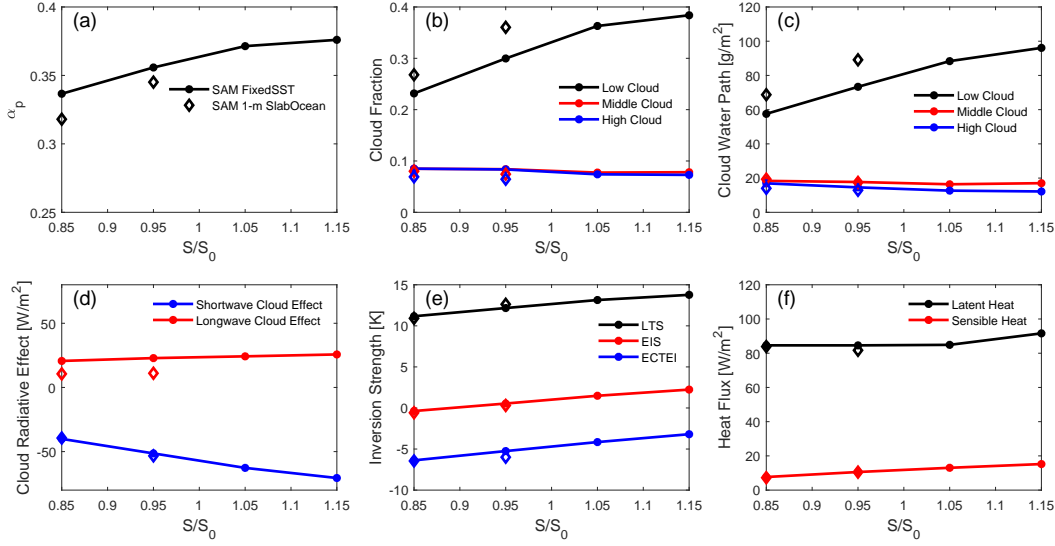


Figure 3. Same as Figure 2 but for the experiments in which the TOA and surface are nearly energy-balanced. The dot markers represent fixed-SST experiments, and the diamond markers represent slab ocean experiments.

(2021) are higher than those shown here, because the effect of varying solar constant on the value of shortwave cloud radiative effect without the changes of clouds was not excluded.

Moreover, the temperature patterns and the trends of cloud-related variables are in line with the CAM4 simulations in Goldblatt et al. (2021) (Figures S5 and S6). However, there are still some differences. For example, the change of high-level cloud fraction in CAM4 is larger than that in SAM (Figures 2b and S5b). Besides, cloud water paths in our simulations are lower than that in CAM4. The high-level cloud water path in SAM decreases from $0.70S_0$ to $1.00S_0$, but CAM4 shows an opposite trend (Figures 2c and S5c). The planetary albedo here is larger (Figure 2a), and the magnitude of the shortwave cloud radiative effect is also larger (Figures 2d and S5d).

Changing insolation and CO_2 concentration synchronously can also lead to changes in atmospheric temperature, atmospheric circulation, and cloud pattern. When we increase the insolation and meanwhile decrease the CO_2 concentration, the lower atmosphere becomes cooler but the upper atmosphere becomes warmer (Figure 5d), the subsidence branch of the Hadley circulation becomes weaker (Figure 5e), and the low-level clouds increase at almost every latitude (Figure 5f). These patterns are similar to that in CAM4 shown in Goldblatt et al. (2021). But, the patterns in our simulations are more symmetric between the northern and southern hemispheres due to the aquaplanet we use.

3.2 Mechanisms for Low-level Cloud Feedback

Increasing insolation but meanwhile decreasing CO_2 concentration leads to the change of radiative heating rate, which can cause the change of clouds through several processes. Importantly, the lower troposphere experiences radiative cooling, but the upper troposphere experiences radiative warming (Figures 5h and 5i), and subsequently the lower troposphere becomes cooler but the upper troposphere becomes warmer (Figures 5d and 5g). To examine what factors dominate the changes in the radiative heating rates, we use an off-line radiative transfer model, RRTMG (Mlawer et al., 1997; Clough et al., 2005), to calculate the clear-sky longwave and shortwave heating rates under different conditions (Figure S7). We find that

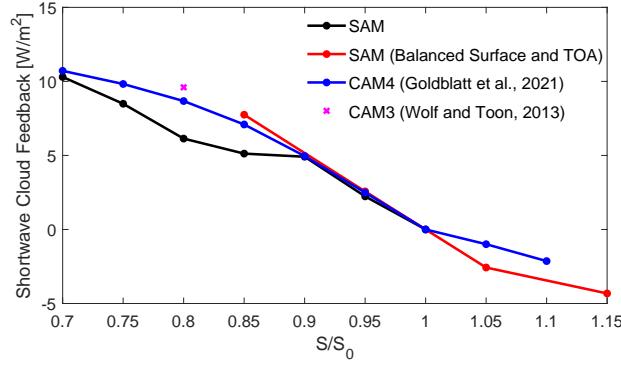


Figure 4. The shortwave cloud feedback in different simulations. The $1.00S_0$ case is chosen as the baseline, so its shortwave cloud feedback is zero. The magenta cross is the data from Wolf and Toon (2013), which used the general circulation model CAM3 but with a modified radiative transfer module.

decreasing CO_2 concentration leads to lower-tropospheric longwave radiative cooling, but the upper-tropospheric longwave heating rate doesn't change significantly (Figure S7b). In our simulations, the changes of water vapor concentration are small, as well as its radiative effects (Figures S7a, d, and e). For shortwave radiative heating rate, the effect of changing solar constant is greater than that of changing CO_2 or H_2O . When the solar radiation is increased, the clear-sky shortwave heating rate increases at all levels (Figure S7f). In short, from $0.70S_0$ to $1.00S_0$, the enhanced lower-tropospheric radiative cooling dominated by less CO_2 and upper-tropospheric radiative warming dominated by more insolation make the lower troposphere and the upper troposphere become cooler and warmer, respectively.

Why there are more low-level clouds from $0.70S_0$ to $1.00S_0$? Following the analyzing methods of previous work (e.g., Bretherton et al. (2013); Bretherton (2015); Qu et al. (2015); Klein et al. (2017); McCoy et al. (2017); Mieslinger et al. (2019)), we find four different processes, including boundary layer inversion, moisture gradient across the inversion, large-scale atmospheric circulation, and sensible heat flux and Bowen ratio. The details are as follows:

Boundary layer inversion. The lower troposphere becomes cooler while the upper troposphere becomes warmer from $0.70S_0$ to $1.00S_0$, so that the strength of the boundary layer inversion increases (Figure 5g). These can also be seen from stability indicators, such as lower tropospheric stability (LTS), estimated inversion strength (EIS), and estimated cloud-top entrainment index (ECTEI) (Slingo (1987); Wood and Bretherton (2006); Kawai et al. (2017); Text S3). All these three indicators show increased inversion strengths at all latitudes (Figures 2e and S8b-d). The stronger inversions can reduce dry air entrainment between the free troposphere and boundary layer and permit more boundary layer clouds (Klein & Hartmann, 1993; Wood & Bretherton, 2006).

Moisture gradient across the inversion. The moisture gradient (δq) across the inversion is characterized by the difference in specific humidity between the surface and 700 hPa. Both air temperature and relative humidity (RH) at 700 hPa increase from $0.70S_0$ to $1.00S_0$, but near-surface temperature and RH nearly do not change (Figures 5g and 5j), which leads to δq gradually decreases (Figure S8e). The smaller specific humidity gradient can lead to less dry entrainment across the inversion, which promotes low-level cloud maintenance (Van der Dussen et al., 2015; Scott et al., 2020; Zhu & Poulsen, 2020).

Large-scale atmospheric circulation. The subsidence branch of the Hadley circulation becomes weaker from $0.70S_0$ to $1.00S_0$ (Figure 5e). The more stable free troposphere (Fig-

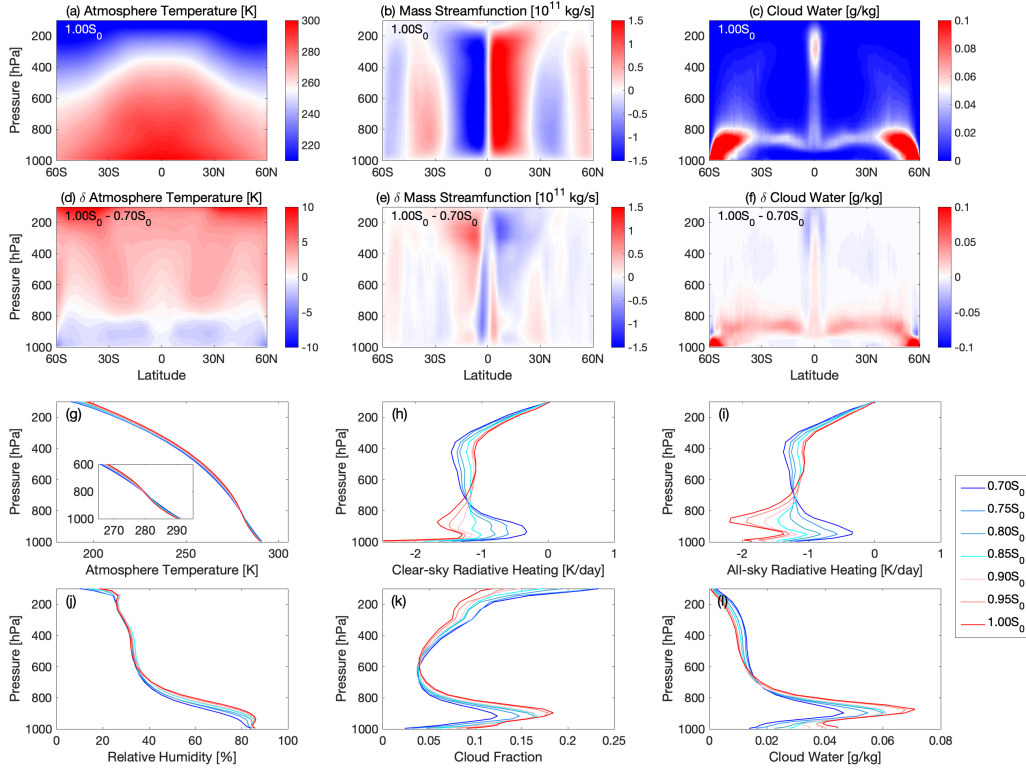


Figure 5. Upper two rows: zonal-mean spatial patterns in the $1.00S_0$ experiment (a–c) and the differences between $1.00S_0$ and $0.70S_0$ (d–f). From left to right, the variables are: atmospheric temperature, meridional mass streamfunction, and cloud water. Lower two rows: global-mean profiles of (g) atmosphere temperature, (h)–(i) clear-sky and all-sky radiative heating rate (shortwave plus longwave), (j) relative humidity, (k) cloud fraction, and (l) cloud water. Note that the cloud fraction in (k) is defined as the fraction of grids with cloud water larger than 0.01 g kg^{-1} (Wyant et al., 2009).

ure 5d) and the increase of static stability in the free troposphere may contribute to the weaker Hadley cells (e.g., Mitas and Clement (2006); Chemke and Polvani (2019)). The weaker subsidence allows the planetary boundary layer to extend to a higher altitude and thereby more low-level clouds can form (Bretherton et al., 2013; Bretherton, 2015).

Sensible heat flux and Bowen ratio. Surface sensible heat flux slightly increases and latent heat flux keeps almost constant from $0.70S_0$ to $1.00S_0$ (Figures 2f and S8f). The larger temperature gradient near the surface layer (Figure 5d) can contribute to larger sensible heat flux, but water vapor concentration near the surface layer which influences the latent heat flux nearly doesn't change (Figure S7a). A larger sensible heat flux can increase the buoyancy and supply more heat from the surface to the boundary layer. Meanwhile, Bowen ratio, which is defined as the ratio of surface sensible heat flux to latent heat flux, increases from $0.70S_0$ to $1.00S_0$ (Figure S9a). It can increase cloud water flux at cloud base, by influencing the efficiency of the heat cycle. Larger Bowen ratio corresponds to larger ratio of mechanical work to generate convection, supporting more low-level clouds (Figure S9b, Sakradzija and Hohenegger (2017); Mieslinger et al. (2019)).

The mechanisms addressed above can also be found in the four added fixed SST experiments and in the two slab ocean experiments (Figures S10 and S11). This implies that our main conclusions are likely robust.

4 Conclusions and Discussions

In this study, we use a near-global cloud-permitting model to re-investigate the cloud feedback on Earth’s long-term climate. We apply the grid spacing of $10\text{ km} \times 14\text{ km}$ over a domain of half of the Earth’s equatorial circumference in longitude and 60°S to 60°N in latitude. When solar radiation increases and meanwhile CO_2 concentration decreases, the change of low-level clouds dominates. The underlying mechanisms are analyzed from four different processes (summarized as Figure S12): boundary layer inversion, moisture gradient across the inversion, large-scale atmospheric circulation, and surface heat flux and Bowen ratio. All these four factors contribute to the increase of low-level clouds.

The shortwave cloud feedback in our simulations can contribute $\approx 6\text{ W m}^{-2}$ or 14% of the energy required to offset a fainter Sun that is 20% dimmer than today. For a 30% dimmer Sun, it can contribute $\approx 10\text{ W m}^{-2}$ or 16%. This shortwave cloud feedback is likely to stabilize Earth’s past or future long-term climate, and its impact is limited but unignorable.

Not only shortwave cloud radiative effect but also longwave cloud radiative effect changes in the experiments, but the magnitude of the former is much larger than the latter (Figure 2d). This is due to the fact that the response of low-level cloud water path is greater than that of the high-level cloud water path (Figures 2c, 5l, and S1d–f). Moreover, the concentration of CO_2 can also influence the strength of the longwave cloud radiative effect. When CO_2 concentration is higher, the longwave absorption spectrum is more saturated, which could lead to a weakening of the longwave cloud radiative effect even if there is no change in cloud properties (Wolf & Toon, 2013). This is likely the reason why the cloud fraction and cloud water path of high-level clouds slightly decrease but the longwave cloud radiative effect slightly increases (Figures 2b–d). Unfortunately, the overlaps between CO_2 and cloud absorption spectra are not in model outputs. If these overlaps were considered, the longwave cloud feedback would be smaller than the change of the longwave cloud radiative effect shown in Figure 2d.

There is no continent distribution in the simulations, which would influence the location of ITCZ, the strength of the Hadley circulation, the surface heat fluxes, and other aspects. Future work should examine the role of land-sea distribution as well as use a dynamical ocean to test the effect of ocean dynamics. If continents are taken into account, other additional factors can affect the low-level cloud amount, such as zonal contrast of SST and horizontal energy transport (Norris & Leovy, 1994; Bretherton et al., 2013; Myers & Norris, 2015).

Accurately resolving the clouds needs a cloud-resolving model with a grid spacing of 4 km or less (Weisman & Klemp, 1997). Therefore, using the horizontal resolution of $\approx 10\text{ km}$ with no cumulus parameterization here may affect the strength of the cloud feedback. Besides, the conclusions of this study are based on a one-moment microphysics scheme, and different microphysics schemes may lead to different results, which needs to be examined in future work.

Acknowledgments

We thank Colin Goldblatt and the anonymous reviewer for their constructive comments. We thank Ji Nie, Yuwei Wang, and Jiachen Liu for their helpful discussions. Jun Yang is supported by the National Natural Science Foundation of China (NSFC) under grants 42075046 and 41888101.

Open Research

The simulation data in this study are archived at <https://doi.org/10.5281/zenodo.6592041>. The output data of CAM4 used for comparisons are included in Goldblatt et al. (2021), which can be accessed from <https://doi.org/10.20383/101.0308>.

References

- Bretherton, C. S. (2015). Insights into low-latitude cloud feedbacks from high-resolution models. *Philosophical Transactions of the Royal Society A: Mathematical, Physical and Engineering Sciences*, 373(2054), 20140415.
- Bretherton, C. S., Blossey, P. N., & Jones, C. R. (2013). Mechanisms of marine low cloud sensitivity to idealized climate perturbations: A single-LES exploration extending the CGILS cases. *Journal of Advances in Modeling Earth Systems*, 5(2), 316–337.
- Bretherton, C. S., & Khairoutdinov, M. F. (2015). Convective self-aggregation feedbacks in near-global cloud-resolving simulations of an aquaplanet. *Journal of Advances in Modeling Earth Systems*, 7(4), 1765–1787.
- Byrne, B., & Goldblatt, C. (2014). Radiative forcings for 28 potential Archean greenhouse gases. *Climate of the Past*, 10(5), 1779–1801.
- Charnay, B., Forget, F., Wordsworth, R., Leconte, J., Millour, E., Codron, F., & Spiga, A. (2013). Exploring the faint young Sun problem and the possible climates of the Archean Earth with a 3-D GCM. *Journal of Geophysical Research: Atmospheres*, 118(18), 10–414.
- Charnay, B., Wolf, E. T., Marty, B., & Forget, F. (2020). Is the faint young Sun problem for Earth solved? *Space Science Reviews*, 216(5), 1–29.
- Chemke, R., & Polvani, L. M. (2019). Opposite tropical circulation trends in climate models and in reanalyses. *Nature Geoscience*, 12(7), 528–532.
- Clough, S., Shephard, M., Mlawer, E., Delamere, J., Iacono, M., Cady-Pereira, K., ... Brown, P. (2005). Atmospheric radiative transfer modeling: A summary of the AER codes. *Journal of Quantitative Spectroscopy and Radiative Transfer*, 91(2), 233–244.
- Collins, W. D., Rasch, P. J., Boville, B. A., Hack, J. J., McCaa, J. R., Williamson, D. L., ... Zhang, M. (2006). The formulation and atmospheric simulation of the Community Atmosphere Model version 3 (CAM3). *Journal of Climate*, 19(11), 2144–2161.
- Feulner, G. (2012). The faint young Sun problem. *Reviews of Geophysics*, 50(2).
- Goldblatt, C., Claire, M. W., Lenton, T. M., Matthews, A. J., Watson, A. J., & Zahnle, K. J. (2009). Nitrogen-enhanced greenhouse warming on early Earth. *Nature Geoscience*, 2(12), 891–896.
- Goldblatt, C., McDonald, V. L., & E., M. K. (2021). Earth’s long-term climate stabilized by clouds. *Nature Geoscience*, 14, 143–150.
- Goldblatt, C., & Zahnle, K. J. (2011). Clouds and the Faint Young Sun Paradox. *Climate of the Past*, 7, 203–220.
- Gough, D. O. (1981). Solar interior structure and luminosity variations. *Solar Physics*, 74, 21–34.
- Hartmann, D. L. (2005). *Global physical climatology*. Elsevier Science.
- Heller, R., Duda, J.-P., Winkler, M., Reitner, J., & Gizon, L. (2021). Habitability of the early Earth: liquid water under a faint young Sun facilitated by strong tidal heating due to a closer Moon. *PalZ*, 95(4), 563–575.
- Kawai, H., Koshiro, T., & Webb, M. J. (2017). Interpretation of factors controlling low cloud cover and low cloud feedback using a unified predictive index. *Journal of Climate*, 30(22), 9119–9131.
- Khairoutdinov, M. F., & Kogan, Y. L. (1999). A large eddy simulation model with explicit microphysics: Validation against aircraft observations of a stratocumulus-topped boundary layer. *Journal of Atmospheric Sciences*, 56(13), 2115–2131.
- Khairoutdinov, M. F., & Randall, D. A. (2003). Cloud resolving modeling of the ARM summer 1997 IOP: Model formulation, results, uncertainties, and sensitivities. *Journal of the Atmospheric Sciences*, 60, 607–625.

- Klein, S. A., Hall, A., Norris, J. R., & Pincus, R. (2017). Low-cloud feedbacks from cloud-controlling factors: A review. *Surveys in Geophysics*, *38*, 1307–1329.
- Klein, S. A., & Hartmann, D. L. (1993). The seasonal cycle of low stratiform clouds. *Journal of Climate*, *6*(8), 1587–1606.
- Le Hir, G., Teitler, Y., Fluteau, F., Donnadieu, Y., & Philippot, P. (2014). The faint young Sun problem revisited with a 3-D climate–carbon model–Part 1. *Climate of the Past*, *10*(2), 697–713.
- McCoy, D. T., Eastman, R., Hartmann, D. L., & Wood, R. (2017). The change in low cloud cover in a warmed climate inferred from AIRS, MODIS, and ERA-Interim. *Journal of Climate*, *30*(10), 3609–3620.
- Mieslinger, T., Horváth, Á., Buehler, S. A., & Sakradzija, M. (2019). The dependence of shallow cumulus macrophysical properties on large-scale meteorology as observed in aster imagery. *Journal of Geophysical Research: Atmospheres*, *124*(21), 11477–11505.
- Mitas, C. M., & Clement, A. (2006). Recent behavior of the Hadley cell and tropical thermodynamics in climate models and reanalyses. *Geophysical Research Letters*, *33*(1).
- Mlawer, E. J., Taubman, S. J., Brown, P. D., Iacono, M. J., & Clough, S. A. (1997). Radiative transfer for inhomogeneous atmospheres: RRTM, a validated correlated-k model for the longwave. *Journal of Geophysical Research: Atmospheres*, *102*(D14), 16663–16682.
- Myers, T. A., & Norris, J. R. (2015). On the relationships between subtropical clouds and meteorology in observations and CMIP3 and CMIP5 models. *Journal of Climate*, *28*(8), 2945–2967.
- Norris, J. R., & Leovy, C. B. (1994). Interannual variability in stratiform cloudiness and sea surface temperature. *Journal of climate*, *7*(12), 1915–1925.
- Pierrehumbert, R. T. (2010). *Principles of planetary climate*. Cambridge University Press.
- Qu, X., Hall, A., Klein, S. A., & DeAngelis, A. M. (2015). Positive tropical marine low-cloud cover feedback inferred from cloud-controlling factors. *Geophysical Research Letters*, *42*(18), 7767–7775.
- Rosing, M. T., Bird, D. K., Sleep, N. H., & Bjerrum, C. J. (2010). No climate paradox under the faint early Sun. *Nature*, *464*(7289), 744–747.
- Sagan, C., & Mullen, G. (1972). Earth and Mars: evolution of atmospheres and surface temperatures. *Science*, *177*, 52–56.
- Sakradzija, M., & Hohenegger, C. (2017). What determines the distribution of shallow convective mass flux through a cloud base? *Journal of the Atmospheric Sciences*, *74*(8), 2615–2632.
- Scott, R. C., Myers, T. A., Norris, J. R., Zelinka, M. D., Klein, S. A., Sun, M., & Doelling, D. R. (2020). Observed sensitivity of low-cloud radiative effects to meteorological perturbations over the global oceans. *Journal of Climate*, *33*(18), 7717–7734.
- Slingo, J. (1987). The development and verification of a cloud prediction scheme for the ECMWF model. *Quarterly Journal of the Royal Meteorological Society*, *113*(477), 899–927.
- Soden, B. J., & Held, I. M. (2006). An assessment of climate feedbacks in coupled ocean–atmosphere models. *Journal of Climate*, *19*, 3354–3360.
- Van der Dussen, J., De Roode, S., Dal Gesso, S., & Siebesma, A. (2015). An LES model study of the influence of the free tropospheric thermodynamic conditions on the stratocumulus response to a climate perturbation. *Journal of Advances in Modeling Earth Systems*, *7*(2), 670–691.
- Vial, J., Bony, S., Stevens, B., & Vogel, R. (2017). Mechanisms and model diversity of trade-wind shallow cumulus cloud feedbacks: a review. *Surveys in Geophysics*, *38*(6), 1331–1353.
- Weisman, W. C., M. L. and Skamarock, & Klemp, J. B. (1997). The resolution dependence of explicitly modeled convective systems. *Monthly Weather Review*, *125*, 527–548.
- Wolf, E., & Toon, O. (2013). Hospitable Archean climates simulated by a general circulation model. *Astrobiology*, *13*(7), 656–673.

- Wood, R., & Bretherton, C. S. (2006). On the relationship between stratiform low cloud cover and lower-tropospheric stability. *Journal of climate*, 19(24), 6425–6432.
- Wordsworth, R., & Pierrehumbert, R. (2013). Hydrogen-nitrogen greenhouse warming in Earth’s early atmosphere. *science*, 339(6115), 64–67.
- Wyant, M. C., Bretherton, C. S., & Blossey, P. N. (2009). Subtropical low cloud response to a warmer climate in a superparameterized climate model. Part I: regime sorting and physical mechanisms. *Journal of Advances in Modeling Earth Systems*, 1(3).
- Zhu, J., & Poulsen, C. J. (2020). On the increase of climate sensitivity and cloud feedback with warming in the Community Atmosphere Models. *Geophysical Research Letters*, 47(18), e2020GL089143.

References From the Supporting Information

References

- Goldblatt, C., McDonald, V. L., & E., M. K. (2021). Earth’s long-term climate stabilized by clouds. *Nature Geoscience*, 14, 143–150.
- Kawai, H., Koshiro, T., & Webb, M. J. (2017). Interpretation of factors controlling low cloud cover and low cloud feedback using a unified predictive index. *Journal of Climate*, 30(22), 9119–9131.
- MacVean, M., & Mason, P. (1990). Cloud-top entrainment instability through small-scale mixing and its parameterization in numerical models. *Journal of Atmospheric Sciences*, 47(8), 1012–1030.
- Slingo, J. (1987). The development and verification of a cloud prediction scheme for the ECMWF model. *Quarterly Journal of the Royal Meteorological Society*, 113(477), 899–927.
- Wood, R., & Bretherton, C. S. (2006). On the relationship between stratiform low cloud cover and lower tropospheric stability. *Journal of climate*, 19(24), 6425–6432